Int. J. Nanosci. Nanotechnol., Vol. 12, No. 4, Dec. 2016, pp. 233-241

Preparation and Characterization of Reduced Graphene Oxide Doped in Sol-Gel Derived Silica for Application in Electrochemical Double-Layer Capacitors

Rahim Mohammad-Rezaei*, Habib Razmi

Department of Chemistry, Faculty of Sciences, Azarbaijan Shahid Madani University, P.O.Box 53714-161, Tabriz, Iran

(*) Corresponding author: r.mohammadrezaei@azaruniv.edu
(Received: 26 June 2015 and Accepted: 08 August 2016)

Abstract

In this study, a new graphene ceramic composite (GCC) was prepared based on the reduced graphene oxide (rGO) doped in sol-gel derived silica. The GCC was prepared by dispersing rGO nanosheets into the sol-gel precursors containing methyl triethoxysilane, methanol and hydrochloric acid solution. During an acid catalyzed hydrolyze reaction and gelation process, rGO nanosheets were successfully doped into the prepared gel. The fabricated GCC was characterized by field emission scanning electron microscopy, Transmission electron microscopy, Fourier transform infrared spectroscopy, X-ray diffraction, thermogravimetric analysis, cyclic voltammetry and galvanostatic charge/discharge techniques. According to the electrochemical results, the prepared GCC has shown remarkable specific capacitance in comparison with carbon ceramic composite. Due to unique configuration of GCC and large specific surface area of rGO, the resultant GCC shows specific capacitance of 428 F g^{-1} at current density of 1 A g^{-1} and good cycling stability using three electrode system.

Keywords: *Graphene, Sol-gel, Double layer capacitor.*

1. INRODUCTION

There are a lot of research interests in the development of energy storage devices. Supercapacitors or electrochemical double-layer capacitors (EDLCs) store and release electrical energy based on the electrolyte ions which forming an electric double layer at the interface of electrodes and electrolyte [1-3]. Currently, the development of new materials with higher specific power density, faster charge/discharge rate, and longer lifetime has been very attractive. Carbonaceous material, such as carbon nanotubes, activated carbon, mesoporous carbon, and carbon aerogels have been studied as electrode materials for electrochemical supercapacitors [4-9].

Graphene is a new generation of carbon allotropes with two-dimensional single-layer of carbon sheets and a hexagonal packed lattice structure that shows unique physicochemical properties such as high conductivity, good mechanical strength, high surface to volume ratio and great chemical stability [9]. Recently graphene nanosheets and its composites such as metal oxide/graphene and polymer/graphene have been used as a suitable material for supercapacitor applications [10-14]. Although these composites represent high specific capacitance, however aggregation of graphene nanosheets during the charge/discharge process, and also weak chemical and mechanical stability of the fabricated composite limits their practical applications.

Sol-gel process involves the manufacturing of inorganic matrices through the formation of colloidal suspension (sol) and gelation of the sol to form a wet gel, which after drying forms the dry gel state (xerogel) [15,16]. During the hydrolysis of alkoxysilanes in sol-gel process, polycondensation of alkoxysilanes occurs. This media is favorable for dispersion of carbonaceous material for preparation of electrochemical devices [17-20]. Considering the simplicity, low cost and practicability of the sol-gel technique, and also the progressive growth of graphene applications, a new electrochemical supercapacitor based on the graphene nanosheets doped in sol-gel derived silica could be developed.

In this study reduced graphene oxide (rGO) was successfully doped into a sol-gel matrix and the resultant composite (GCC) was coated on glassy carbon electrode surface for electrochemical double-layer capacitor applications. Due to the large specific surface area, high electrical conductivity, and unique configuration of the GCC, the resultant composite shows high specific capacitance in comparison with carbon ceramic composite.

2. EXPERIMENT

2.1. Chemicals and apparatus

Methyl triethoxysilane, methanol, hydrochloric acid, and graphite fine powder were purchased from Merck (Darmstadt, Germany; www.merckgroup.com). All other chemicals were of analytical grade and were used without further purification. Double distilled water was used throughout the all experiments.

The electrochemical experiments were carried out using an AUTOLAB PGSTAT-100 (potentiostat/galvanostat) at room temperature. The morphology studies were performed by field emission scanning electron microscopy (FESEM) (Hitachi, model S-4160). X-ray powder diffraction (XRD) patterns were recorded on Brucker AXF (D8 Advance) X-ray power diffractometer with a CuKα radiation source (λ= 0.154056 nm) generated at 40 kV and 35 mA. Thermogravimetric analysis (TGA) curves were obtained on a TGA/SDTA 851 calorimeter at heating and cooling rates of 10 $^{\circ}C\ min^{-1}$ under N_2 atmosphere. Transmission electron microscopy (TEM) image was recorded with Philips CM-10 (Eindhoven, The Netherlands).

2.2. Preparation of hydrothermally reduced graphene oxide powder

Graphene oxide was synthesized from natural flake graphite by modified Hummers method [21]. First, 5 g natural graphite, 3.75 g $NaNO_3$ (99%, Aldrich) and 310 mL H_2SO_4 were mixed in a Pyrex reactor with a water cooling system. This mixture was then stirred for 30 min. Next, 22.5 g $KMnO_4$ was carefully added to this mixture for 1 h. The resultant mixture was stirred for 5 days at room temperature. Then 150 mL of H_2O_2 (30%) was added to the mixture. Upon centrifugation, the GO slurry at the bottom was washed with a 0.5% H_2O_2 solution and then rewashed with deionized water. The dried brown color GO powder mounted on a crucible and was introduced into a quartz furnace and thermally treated at 200 $^{\circ}C$ for 2 h with a heating rate of 5 $^{\circ}C\ min^{-1}$ in a nitrogen atmosphere. The obtained black reduced graphene oxide powder was stable and used without further purification.

2.3. Preparation of graphene doped in sol-gel derived silica

0.15 g of rGO powder was added to the sol suspension containing 0.6 mL methyl triethoxysilane, 0.6 mL hydrochloric acid 0.1 M, and 0.9 mL methanol. The suspension of sol-graphene was shacked for 30 min. During the shaking step, which acid catalyzed hydrolysis reaction of methyl triethoxysilane was occurred, the soft suspension of sol-graphene turned to a rigid gel-graphene composite. Finally the prepared composite was dried overnight

under ambient conditions (25 °C) which finally was called graphene ceramic composite (GCC). In order to compare the electrochemical behavior of GCC with carbon ceramic composite (CCC), the latter was prepared similar to the GCC and just graphite powder was used against rGO [22].

2.4. Electrochemical measurements

The electrochemical performance of the GCC was studied by cyclic voltammetry (CV) and galvanostatic charge/discharge (CD) techniques. The specific capacitance was extracted from both the CV and the galvanostatic CD curves. All the electrochemical measurements were carried out using three-electrode system which was composed of saturated (KCl 3 M) calomel electrode (SCE) as reference electrode, platinum wire as auxiliary electrode, and glassy carbon electrode (GCE) modified with GCC and CCE as working electrode. Prior to modification, the GCE (diameter of 3 mm) was polished using alumina powder and then was ultrasonicated in ethanol and double distilled water for 5 min respectively. Modification of GCE with GCC was as follow: 10 mg of GCC was dispersed into 5 mL ethanol solution followed by 10 min sonication. Then 10 µL of GCC ink was casted on the GCE. This enabled a 20 µg loading of the GCC onto the electrode. Finally the electrodes were dried in air and then 10 µL of 0.05% (v/v) Nafion was casted on the electrode surface which was allowed to dry in air (25 °C). The GCE were modified with CCC as the same procedure.

3. RESULTS AND DISCUSSION

3.1. Characterization of graphene ceramic composite

Considering the hydroxyl groups of hydrothermally reduced graphene oxide (G-OH), and silanol (Si-OH) groups of methyl triethoxysilane, the fallowing reactions could be occurred during the hydrolysis process of methyl triethoxysilane in the presence of rGO; Firstly the acid catalyzed hydrolysis reaction of methyl triethoxysilane occurs (Eq. 1) [23,24]:

$$\equiv Si - OR + H_2O \longrightarrow \equiv Si - OH + ROH$$

(Hydrolysis reaction) (Eq.1)

which could be followed by condensation (Eq. 2 and 3) and/or reaction with hydroxyl groups of graphene (Eq. 4):

$$\equiv Si - OH + RO - Si \equiv \longrightarrow \equiv Si - O - Si \equiv + ROH$$

(Alchol condensation) (Eq. 2)

$$\equiv Si - OH + HO - Si \equiv \longrightarrow \equiv Si - O - Si \equiv + H_2O$$

(Water condensation) (Eq. 3)

$$\equiv Si - OH + G - OH \equiv \longrightarrow \equiv Si - O - G + H_2O$$

(Eq. 4)

Also the following reaction could be occurred at the surface of graphene:

$$G - OH + \equiv Si - O - Si \equiv \longrightarrow G - O - Si \equiv + SiOH$$

(Eq. 5)

$$G - OH + RO - Si \equiv \longrightarrow G - O - Si \equiv + ROH$$

(Eq. 6)

Fig. 1 shows the FTIR spectra of the hydrothermally reduced graphene oxide and GCC. A broad adsorption band on the rGO and GCC structures appeared at 3000-3500 cm^{-1} is related to the hydroxyl group [25]. In the FTIR spectrum of rGO there is a small peak in 1718 cm^{-1} which could be due to the presence of slight carbonyl groups in graphene. The C=C stretching from the skeletal vibration in the un-oxidized graphitic domain was observed at 1617 cm^{-1}. Also O-H bending vibrations from the hydroxyl groups were observed at 1384 cm^{-1} in rGO [26, 27]. In the case of GCC, the strong bands at 1027 cm^{-1} and 1111 cm^{-1} were associated with the stretching of the C−O and (Si−O−C/Si−O−Si) asymmetric stretching respectively. The peak at 764 cm^{-1} was

assigned to the stretching vibration of Si-OH. Also, the peak at 1381 cm^{-1} is attributed to the O-H bending vibrations from the hydroxyl groups. The peak at 1272 cm^{-1} is related to stretching vibration of Si-CH_3.

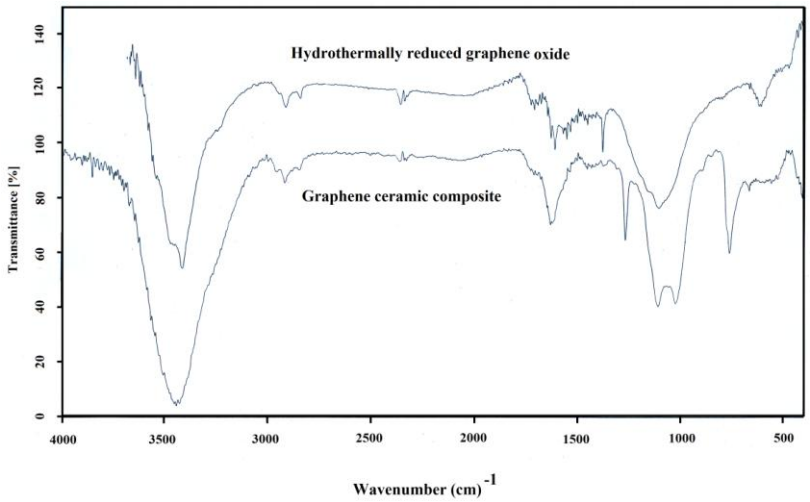

Figure 1. *FTIR spectra of hydrothermally reduced graphene oxide and graphene ceramic composite.*

The morphology of GCC was studied with TEM and FESEM techniques.

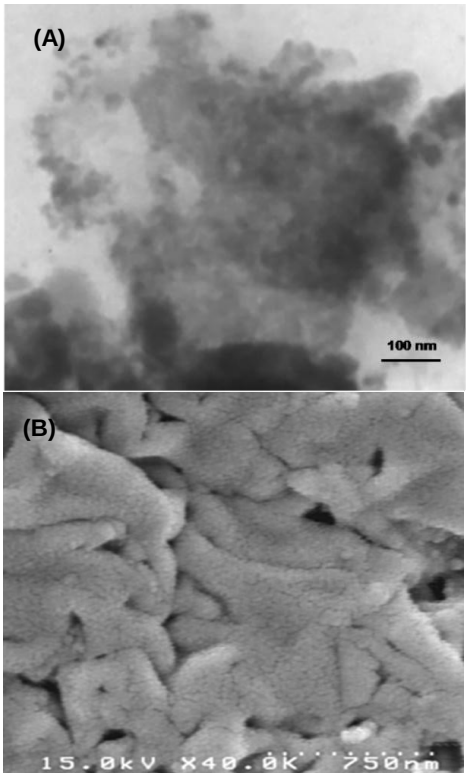

Figure 2. *(A) TEM image of powdered GCC, (B) FESEM image of GCC with 60000 magnification.*

According to TEM image (Fig. 2A) it could be seen that silicone is appropriately decorated on rGO sheets. Also the FESEM of GCC (Fig. 2B) shows that the edges and planes of graphene nanosheets are covered by silicone nanoparticles uniformly. Covering of rGO with silicone nanoparticles decreases the aggregation of rGO nanosheets during charge/discharge process and results GCC with a long cycling stability. The silicone nanoparticles size in this study (acid catalyzed hydrolysis reaction) is smaller than that those reported in the base catalyzed reaction which was reported previously by Zhang and et al [27].

The XRD patterns of exfoliated graphene oxide (A), rGO (b), and GCC (C) were shown in Fig. 3. As can be seen, the XRD pattern of graphene oxide showing a peak at 2θ =9.56 corresponding to a d-spacing of 8.91 nm. This peak could be assigned to the (001) reflection peak of graphite oxide and might depend on the method of preparation and on the number of layers of water in the gallery space of the graphene oxide [28]. When graphene oxide was hydrothermally reduced to graphene, the peak of graphene oxide stacking

disappeared and a new and broad peak at 2θ=24.2˚ (002) appeared confirming the reduction of graphene oxide to graphene. In the case of GCC, the broadening of graphene (002) peak is due to the dominant effect of silica. Also the broad peak at 2θ=11.3˚ corresponding to the amorphous structure of silicone rubber [29, 30].

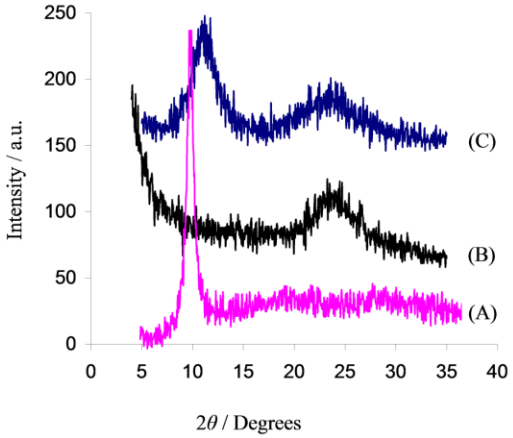

Figure 3. *XRD patterns of graphene oxide (A), hydrothermally reduced graphene oxide (B) and graphene ceramic composite (C).*

Considering the FESEM images and XRD patterns, it could be concluded that graphene nanosheets were appropriately covered by silicone rubber nanoparticles in GCC.

3.2. Thermal properties of graphene ceramic composite

Fig. 4 shows the TGA curves of silica network (prepared with sol-gel method) and GCC heated in a TGA instrument to 800 °C at a heating rate 5 °C min^{-1} under N_2 atmosphere. A mass loss at about 80 °C is due to the removal of adsorbed water. A small mass loss at 200 °C should be assigned to the decomposition of the oxygen containing groups. The weight loss from 550 °C is caused by the pyrolysis of the silane moieties of GCC. Moreover, high temperature pyrolysis of GCC is similar to graphite around 650 °C and attributed to pyrolysis of the carbon skeleton of GCC [39]. In comparison with GCC, silica network has more thermal stability which could be due to absence of graphene and its functional groups. Although silica network is more thermally stable than GCC, however silica network is not suitable for electrochemical double-layer capacitors.

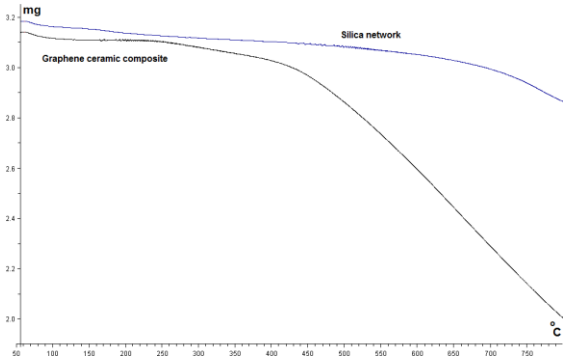

Figure 4. *TGA curves of graphene ceramic composite (lower curve) and silica network (upper curve).*

3.3. Electrochemical behavior of graphene ceramic composite

In order to calculate effective surface area of graphene ceramic composite (GCC) and carbon ceramic composite (CCC), cyclic voltammetries of GCC|GCE and CCC|GCE were investigated in 5 mM $K_3[Fe(CN)_6]$ and 0.1 M of KNO_3 solution in scan rate of 50 mV s^{-1} (not shown). By using Randles-Sevcik equation, the effective surface area of GCC was calculated 2.82×10^{-3} cm^2 in comparison with CCC which calculated as 1.23×10^{-4} cm^2.

The electrochemical behavior of GCC and CCC were investigated by CV and CD techniques in 1.0 M aqueous Na_2SO_4 electrolyte using a three-electrode system on the glassy carbon electrode (GCE). Fig. 5A indicates the CV curves of GCC|GCE (curve a) and CCC|GCE (curve b) at a scan rate of 100 mV s^{-1} in the potential range 0.0 to 1.0 V, which showing no faradic peak in the working potential window of the electrodes. From the CV curves, it could be observed that the GCC|GCE has larger voltammetric current responses in comparison with CCC|GCE, revealing

higher charge storage capability of GCC|GCE. As the integrated area under the CV curve within the potential window indicates the energy density, GCC|GCE has an enhanced energy density than that of CCC|GCE. Fig. 5B shows the CV curves of the GCC|GCE at different scan rates varying from 10 to 120 mV s^{-1}. As can be seen, the CV curves at all scan rates are nearly rectangular shape which is typical for the pure capacitive characteristic, indicating the excellent capacitive behavior and fast charging/discharging processes of the GCC|GCE [31, 32]. According to Eq. (7), the specific capacitances of the CV curves at different scan rates were calculated by integrating the CV curves to obtain the charge (Q) and then dividing by the mass of electrode materials (m), the scan rate (v) and the potential window ($\Delta V = V_a - V_c$) [33]:

$$C_S = \frac{Q}{m\,\Delta V} = \frac{1}{mv\,(V_a - V_c)} \int_{V_a}^{V_c} I\,(V)\,dV \qquad \text{(Eq. 7)}$$

Fig. 5C shows the variation in the specific capacitance of GCC|GCE as a function of scan rates. It could be found that the specific capacitance decreases with the increase of scan rates from 10 to 120 mV s^{-1}. The decrease of specific capacitance with increasing the scan rates is due to the relative long diffusion length for the GCC structure and an increase of the ion transport related resistance.

Galvanostatic charge-discharge method was also used to evaluate the capacitance behavior of the GCC|GCE. Fig. 6 shows the galvanostatic CD curves of GCC|GCE with a potential range from 0.0 to 1.0 V at different current densities of 1 A g^{-1}, 3 A g^{-1}, 4 A g^{-1}, 5 A g^{-1}, and 10 A g^{-1}. The curves behave as triangular during the charge-discharge process within all the potential range, proving good charge-discharge reversibility and perfect capacitive behavior of the supercapacitor.

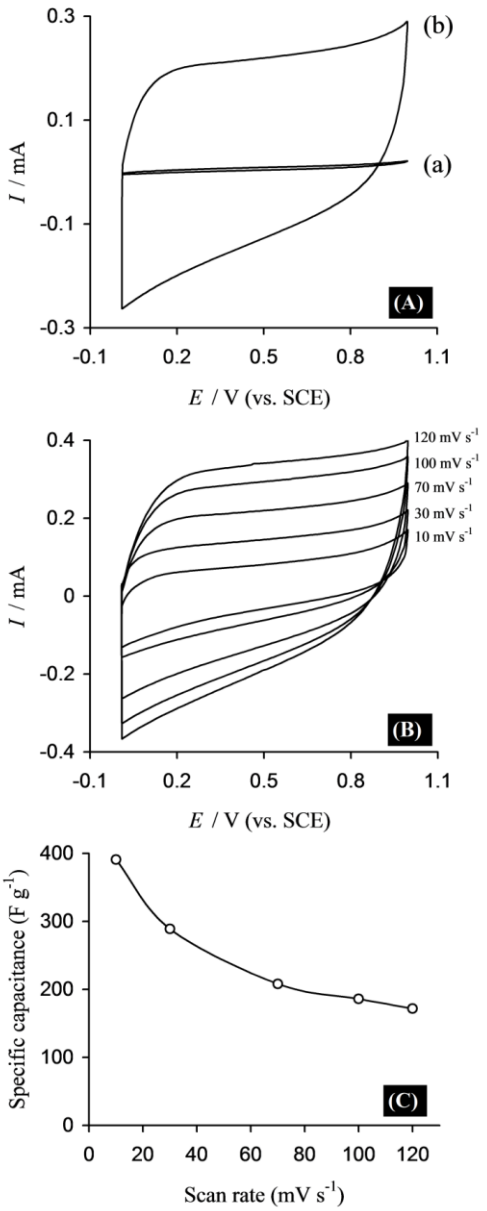

Figure 5. *(A) CV curves of GCC|GCE (a) and CCC|GCE (b) in 1.0 M aqueous Na_2SO_4 solution; scan rate 50 mV s^{-1}. (B) CV curves of GCC|GCE at different scan rates; 10 (a), 30 (b), 70 (c), 100 (d), and 120 (e) mV s^{-1}. (C) Plot of specific capacitance of GCC|GCE as a function of scan rate.*

The specific capacitance was calculated from the slope of galvanostatic CD curves using Eq. 8 [34]:

$$C_S = \frac{I}{m \times \frac{dV}{dt}} \qquad \text{(Eq. 8)}$$

where I is the applied current, m is the mass of the active material, and $\frac{dV}{dt}$ is the absolute value of the slope of the discharging curve. The specific capacitance of the GCC is remarkably increased in comparison with that of CCC. Specific capacitances of 428, 375, 314, 271, and 250 F g^{-1} have been achieved for the GCC electrode at current densities of 1 A g^{-1}, 3 A g^{-1}, 4 A g^{-1}, 5 A g^{-1}, and 10 A g^{-1} respectively, which are remarkably higher than those reported previously for graphene based electrodes [35-38].

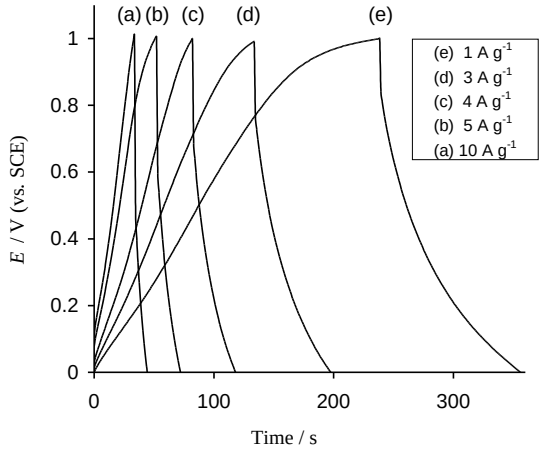

Figure 6. *(A) Galvanostatic CD curves of GCC|GCE at constant current densities of 1 A g^{-1}, 3 A g^{-1}, 4 A g^{-1}, 5 A g^{-1} and 10 A g^{-1}*

The superior performance of the GCC could be attributed to the uniform distribution of graphene nanosheets, high active surface area and presence of silicon rubber nanoparticles which enabling the graphene nanosheets to remain in atomic layer structure and high surface area. Finally the unique morphology of GCC could supply enhanced accessibility to the electrolyte ions resulting an enhancement of the EDLC capacitance.

The cycle stability of supercapacitors is important for its practical applications. In order to evaluate the cycling stability of the GCC, CV studies were performed at a scan rate of 100 mV s^{-1} between 0.0 V and 1.0 V in 1.0 M Na_2SO_4 electrolyte. The long-cycle performance is shown in Fig. 7, and the CV curves of the first and 2000th cycles are shown as an inset.

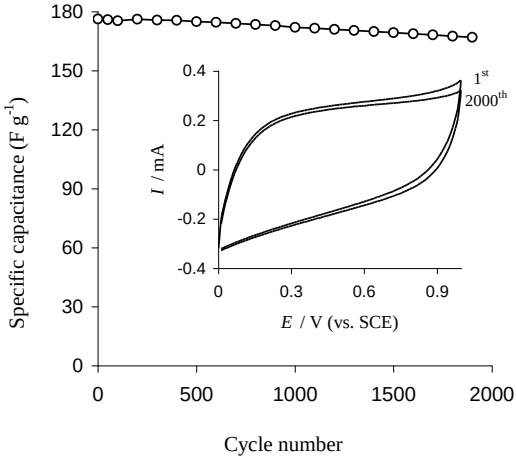

Figure 7. *Variation of the specific capacitance of GCC|GCE as a function of cycle number measured at 100 mV s^{-1} in 1.0 M Na_2SO_4 aqueous solution (the inset shows the CV curves of the 1st and the 2000th cycles).*

After 2000 cycles, the specific capacitance of GCC|GCE remained 94.5% (167 F g^{-1}) of its initial capacitance proving appropriate cycling stability of the electrode. The presence of silicone rubber nanoparticles which uniformly distributed on the plane and edges of graphene nanosheets, prevent the aggregation of graphene sheets during the long term usage. Also good cycling stability of the GCC could be attributed to the double layer capacitance brought by graphene nanosheets and efficient electron transfer channels from the graphene.

4. CONCLUSION

In summary, a new graphene ceramic composite based on the acid catalyzed hydrolysis reaction of methyl triethoxysilane in the presence of hydrothermally reduced graphene oxide was prepared. To the best of our knowledge, this is the first report in preparation of graphene ceramic composite and application as an efficient electrochemical double-layer capacitor. The GCC represents appropriate cycling

stability and high capacitance using cyclic voltammetry and charge/discharge galvanostatic techniques.

ACKNOWLEDGEMENT

The authors gratefully acknowledge The Research Council of Azarbaijan Shahid Madani University for financial support.

REFERENCES

1. Kotz, R., Carlen, M., (2000). "Principles and applications of electrochemical capacitors", *Electrochim. Acta*, 45: 2483-2498.
2. Wang, G., Zhang, L., Zhang, J., (2012). "A review of electrode materials for electrochemical supercapacitors", *Chem. Soc. Rev.*, 4: 797-828.
3. Hosseini, M. G., Shahryari, E., Najjar, R., Ahadzadeh, I., (2015). "Study of Super Capacitive Behavior of Polyaniline/manganese Oxide-Carbon Black Nanocomposites Based Electrodes", *Int. J. Nanosci. Nanotechnol.*, 11: 147-157.
4. Frackowiak, E. Beguin, F., (2002). "Electrochemical storage of energy in carbon nanotubes and nanostructured carbons", *Carbon*, 40: 1775-1787.
5. Zhang, L. L., Zhao, X. S., (2009). "Carbon-based materials as supercapacitor electrodes", *Chem. Soc. Rev.*, 38: 2520-2531.
6. Xia, K., Gao, Q., Jiang, J., Hu, J., (2008). "Hierarchical porous carbons with controlled micropores and mesopores for supercapacitor electrode materials", *Carbon*, 46: 1718-1726.
7. Nandhini, R., Mini, P. A., Avinash, B., Nair, S. V., Subramanian, K. R. V., (2012). "Supercapacitor electrodes using nanoscale activated carbon from graphite by ball milling", *Mater. Lett.*, 87: 165-168.
8. Fan, X., Yu, C., Ling, Z., Yang, J., Qiu, J., (2013). "Hydrothermal Synthesis of Phosphate-Functionalized Carbon Nanotube-Containing Carbon Composites for Supercapacitors with Highly Stable Performance", *ACS Appl. Mater. Interfaces*, 5: 2104-2110.
9. Novoselov, K. S., Geim, A. K., Morozov, S. V., Jiang, D., Zhang, Y., Dubonos, S. V., Grigorieva, I. V., Firsov, A. A., (2004). "Electric Field Effect in Atomically Thin Carbon Films", Science, 306: 666-669.
10. Wang, Z. L., Xu, D., Wang, H. G., Wu, Z., Zhang, X. B., (2013). "In situ fabrication of porous graphene electrodes for high-performance energy storage", *ACS Nano*, 7: 2422-2430.
11. Peng, X.,Y., Liu, X. X., Diamond, D., Lau, K. T., (2011). "Synthesis of electrochemically-reduced graphene oxide film with controllable size and thickness and its use in supercapacitor", *Carbon*, 49: 3488-3496.
12. Xiang, C., Li, M., Zhi, M., Manivannan, A., Wu, N., (2013) "A reduced graphene oxide/Co_3O_4 composite for supercapacitor electrode", *J. Power Sources*, 226: 65-70.
13. Wei, W., Cui, X., Chen, W., Ivey, D.G., (2011). "Manganese oxide-based materials as electrochemical supercapacitor electrodes", *Chem. Soc. Rev.* 40: 1697-1721.
14. Li, J., Xie, H., (2012). "Synthesis of graphene oxide/polypyrrole nanowire composites for supercapacitors", *Mater. Lett.*, 78: 106-109.
15. Hench, L. L., West, J. K., (1990). "The sol-gel process", *Chem. Rev*., 90: 33-72.
16. Tohidi, S. H., Novinrooz, A. J., Derhambakhsh, M., Grigoryan, G. L. (2012). "Dependence of Spectroscopic Properties of Copper Oxide Based Silica Supported Nanostructure on Temperature", 8: 143-148.
17. Gong, K., Zhang, M., Yan, Y., Su, L., Mao, L., Xiong, S., Chen, Y., (2004). "Sol-Gel-Derived Ceramic-Carbon Nanotube Nanocomposite Electrodes: Tunable Electrode Dimension and Potential Electrochemical Applications", *Anal. Chem*., 76: 6500-6505.
18. Oskam, G., Searson, P.,C., (1998). "Sol-Gel Synthesis and Characterization of Carbon/Ceramic Composite Electrodes", *J. Phys. Chem. B*, 102: 2464-2468.
19. Wang, Q., Lu, G., Yang, G., (2004). "Myoglobin/Sol-Gel Film Modified Electrode: Direct Electrochemistry and Electrochemical Catalysis", *Langmuir*, 20: 1342-1347.
20. Ravi Shankaran, D., Uehara, N., Kato, T., (2003). "Sol-gel derived metal dispersed ceramic–graphite composite electrode for amperometric determination of dopamine", *Anal. Chim. Acta*, 478: 321-327.
21. Xu, Y., Bai, H., Lu, G., Li, C., Shi, G., (2008). "Flexible Graphene Films via the Filtration of Water-Soluble Noncovalent Functionalized Graphene Sheets", *J. Am. Chem. Soc*., 130: 5856-5857.
22. Tslonsky, M., Gun, G., Glezer, V., Lev, O., (1994). "Sol-Gel-Derived Ceramic-Carbon Composite Electrodes: Introduction and Scope of Applications", *Anal. Chem*., 66: 1747-1753.
23. Jeong, H. K., Lee, Y. P., Jin, M. H., Kim, E. S., Bae, J. J., Lee, Y. H., (2009). "Thermal stability of graphite oxide", *Chem. Phys. Lett*., 470: 255-258.
24. Botas, C., Alvarez, P., Blanco, C., Santamaria, R., Granda, M., Gutierrez, M. D., Rodriguez-Reinoso, F., Menendez, R., *Carbon*, 52: 476-485.
25. Szabo, T., Berkesi, O., Forgo, P., Josepovits, K., Sanakis, Y., Petridis, D., Dekany, I., (2006). "Evolution of Surface Functional Groups in a Series of Progressively Oxidized Graphite Oxides", *Chem. Mater*., 18: 2740-2749.

26. Li, D., Muller, M.B., Gilje, S., Kaner, R.B., Wallace, G.G., (2008). “Processable aqueous dispersions of graphene nanosheets”, *Nat. Nanotechnol*., 3: 101-105.
27. Zhang, W. L., Choi, H. J., (2012). “Silica-Graphene Oxide Hybrid Composite Particles and Their Electroresponsive Characteristics”, *Langmuir*, 28: 7055-7062.
28. Zhang, K., Zhang, L. L., Zhao, X. S., Wu, J. S., (2010). “Graphene/Polyaniline Nanofiber Composites as Supercapacitor Electrodes”, *Chem. Mater*. 22: 1392-1401.
29. Yang, D., Zhang, W., Jiang, B., (2013). “Ceramization and oxidation behaviors of silicone rubber ablative composite under oxyacetylene flame”, *Ceram. Int*. 39: 1575-1581.
30. Kim, E. S., Kim, E. J., Shim, J. H., Yoon, J. S., (2008). “Thermal stability and ablation properties of silicone rubber composites”, *J. Appl. Polym. Sci*., 110: 1263-1270.
31. Zhou, Z., Wu, X. F., (2013). “Graphene-beaded carbon nanofibers for use in supercapacitor electrodes: Synthesis and electrochemical characterization”, *J. Power Sources*, 222: 410-416.
32. Yan, j., Wei, T., Shao, B., Ma, F., Fan, Z., Zhang, M., Zheng, C., Shang, Y., Qian W., Wei, F., (2010). “Electrochemical properties of graphene nanosheet/carbon black composites as electrodes for supercapacitors”, *Carbon*, 48: 1731-1737.
33. Lee, J. W., Ko, J. M., Kim, J. D., (2012). “Hydrothermal preparation of nitrogen-doped graphene sheets via hexamethylenetetramine for application as supercapacitor electrodes”, *Electrochim. Acta*, 85: 459-466.
34. Fu, C., Kuang, Y., Huang, Z., Wang, X., Yin, Y., Chen, J., Zhou, H., (2011). “Supercapacitor based on graphene and ionic liquid electrolyte”, *J. Solid State Electrochem*., 15: 2581-2585.
35. Liu, S., Ou, J., Wang, J., Liu, X., Yang, S., (2011). “A simple two-step electrochemical synthesis of graphene sheets film on the ITO electrode as supercapacitors”, *J. Appl. Electrochem*., 41: 881-884.
36. Shao, Y., Wang, J., Engelhard, M., Wang, C., Lin, Y., (2010). “Facile and controllable electrochemical reduction of graphene oxide and its applications”, *J. Mater. Chem*., 20: 743-748.
37. Li, Z. J., Yang, B. C., Zhang, S. R., Zhao, C. M., (2012). “Graphene oxide with improved electrical conductivity for supercapacitor electrodes”, *Appl. Surf. Sci.*, 258: 3726-3731.
38. Le, L. T., Ervin, M. H., Qiu, H., Fuchs, B. E., Lee, W. Y., (2011). “Graphene supercapacitor electrodes fabricated by inkjet printing and thermal reduction of graphene oxide”, *Electrochem. Commun*., 13: 355-358.
39. Yang, H., Li, F., Shan, C., Han, D., Zhang, Q., Niu, L., Ivaska, A., (2009). “Covalent functionalization of chemically converted graphene sheets *via* silane and its reinforcement”, *J. Mater. Chem*., 19: 4632-4638.